

## RESEARCH ARTICLE

# Arih2 regulates Hedgehog signaling through smoothed ubiquitylation and ER-associated degradation

Bo Lv<sup>1</sup>, Xiao-Ou Zhang<sup>2</sup> and Gregory J. Pazour<sup>1,\*</sup>**ABSTRACT**

During Hedgehog signaling, the ciliary levels of Ptch1 and Smo are regulated by the pathway. At the basal state, Ptch1 localizes to cilia and prevents the ciliary accumulation and activation of Smo. Upon binding a Hedgehog ligand, Ptch1 exits cilia, relieving inhibition of Smo. Smo then concentrates in cilia, becomes activated and activates downstream signaling. Loss of the ubiquitin E3 ligase Arih2 elevates basal Hedgehog signaling, elevates the cellular level of Smo and increases basal levels of ciliary Smo. Mice express two isoforms of Arih2 with Arih2 $\alpha$  found primarily in the nucleus and Arih2 $\beta$  found on the cytoplasmic face of the endoplasmic reticulum (ER). Re-expression of ER-localized Arih2 $\beta$  but not nuclear-localized Arih2 $\alpha$  rescues the *Arih2* mutant phenotypes. When Arih2 is defective, protein aggregates accumulate in the ER and the unfolded protein response is activated. Arih2 $\beta$  appears to regulate the ER-associated degradation (ERAD) of Smo preventing excess and potentially misfolded Smo from reaching the cilium and interfering with pathway regulation.

**KEY WORDS:** Intraflagellar transport, Hedgehog signaling, Cilia, Ubiquitin

**INTRODUCTION**

The Hedgehog pathway is an evolutionarily conserved signaling cascade that functions in embryonic development and tissue homeostasis. Malfunction of the pathway causes a variety of developmental syndromes and cancers. In vertebrates, this pathway is mediated by cilia, hair-like organelles found on nearly all eukaryotic cells. In brief, in the basal state without sonic hedgehog (SHH) ligand present, the SHH receptor Ptch1 localizes to cilia and inhibits the ciliary accumulation and activation of Smo. Upon binding of the Hedgehog ligand, Ptch1 stops inhibiting Smo, and Ptch1 exits cilia. Uninhibited Smo accumulates in cilia, becomes activated and promotes the activation of the Gli transcription factors, which move to the nucleus to promote gene expression. Our previous work showed that ciliary Smo levels are regulated by ubiquitylation. At the basal state, the ubiquitin E3 ligase Wwp1 localizes to cilia by binding Ptch1. This promotes the ubiquitylation of Smo, which promotes the interaction of Smo with the

intraflagellar transport (IFT) system for removal from cilia (Desai et al., 2020; Lv et al., 2021).

The post-translational modification of proteins by ubiquitylation plays pivotal roles in a wide range of signaling processes (Otten et al., 2021). The covalent attachment of the ubiquitin peptide to a target can change the stability, localization, trafficking, activity and protein–protein interactions of the target. Ubiquitylation requires the activation of ubiquitin by E1 ubiquitin-activating enzymes, the transfer of the ubiquitin to an E2 ubiquitin-conjugating enzyme followed by the ligation of the ubiquitin onto the target protein by an E3 ubiquitin ligase or a complex of E2 and E3 enzymes. There are two E1 activating enzymes, ~40 E2 conjugating enzymes and more than 600 E3 ligases encoded in the human genome.


In this work, we examine the role of Arih2 in regulating Smo. Our prior work showed that loss of Arih2 elevated ciliary Smo levels at the basal state and increased the level of Smo in cells (Lv et al., 2021). Arih2, also known as TRIAD1 is a RING-in-between-RING (RBR) type E3 ubiquitin ligase, has been mostly studied in the context of cancer where it has anti-proliferative effects on myeloid progenitor cells and its expression is reduced in acute myeloid leukemia (Marteijn et al., 2005; Wang et al., 2011). The gene is widely distributed across metazoans. It is found in organisms like mouse and humans, which utilize ciliary Hedgehog signaling, *Drosophila melanogaster*, which has non-ciliary Hedgehog signaling, and organisms like *Caenorhabditis elegans* and *Arabidopsis thaliana*, which do not have Hedgehog signaling. This distribution suggests that Arih2 regulates other pathways besides Hedgehog (Aguilera et al., 2000; Marín and Ferrús, 2002; Mladek et al., 2003). Most mice lacking *Arih2* die perinatally and the few that survive past the first week of life are runty and show signs of excessive inflammation (Lin et al., 2013). The authors of that work did not report phenotypes associated with defective Hedgehog signaling; however, unpublished work from the International Mouse Phenotyping Consortium documents structural birth defects of the heart, kidney, and skin in *Arih2* heterozygotes that might be Hedgehog related (<https://www.mousephenotype.org/data/genes/MGI:1344361>). Vertebrate Arih2 undergoes extensive alternative splicing, producing nine protein variants in human and two in mouse. We find that in mouse, the isoforms are differentially localized, with Arih2 $\alpha$  localized to the nucleus and cytoplasm and Arih2 $\beta$  localized to the endoplasmic reticulum (ER). Only Arih2 $\beta$  rescues the Smo phenotypes in *Arih2*<sup>-/-</sup> cells suggesting the Arih2 $\beta$  controls the biosynthesis of Smo possibly through ER-associated degradation (ERAD).

**RESULTS****Arih2 regulates cellular and ciliary Smo levels**

In a CRISPR-based screen to identify ubiquitin-related genes regulating Hedgehog signaling, we identified the E3 ligase Arih2 as a negative regulator of the pathway, whose loss increased cellular Smo levels and increased Smo ciliary localization (Lv et al., 2021).

<sup>1</sup>Program in Molecular Medicine, University of Massachusetts Medical School, Biotech II, Suite 213, 373 Plantation Street, Worcester, MA 01605, USA. <sup>2</sup>Shanghai Key Laboratory of Maternal and Fetal Medicine, Clinical and Translational Research Center of Shanghai First Maternity and Infant Hospital, Frontier Science Center for Stem Cell Research, School of Life Sciences and Technology, Tongji University, Shanghai, China 200092.

\*Author for correspondence (gregory.pazour@umassmed.edu)

 B.L., 0000-0002-3448-8986; X.-O.Z., 0000-0002-2027-1313; G.J.P., 0000-0002-6285-8796

Handling Editor: Guangshuo Ou  
Received 1 June 2022; Accepted 18 July 2022

In our current work, we seek to understand how *Arih2* regulates the Hedgehog pathway. To ensure that the effect of *Arih2* loss was not limited to our reporter, we assessed the activity of the endogenous

pathway by measuring *Gli1* gene expression (Fig. 1A), which is elevated by pathway activation (Lee et al., 1997). This analysis reproduced our finding that the loss of *Arih2* elevated basal, but not

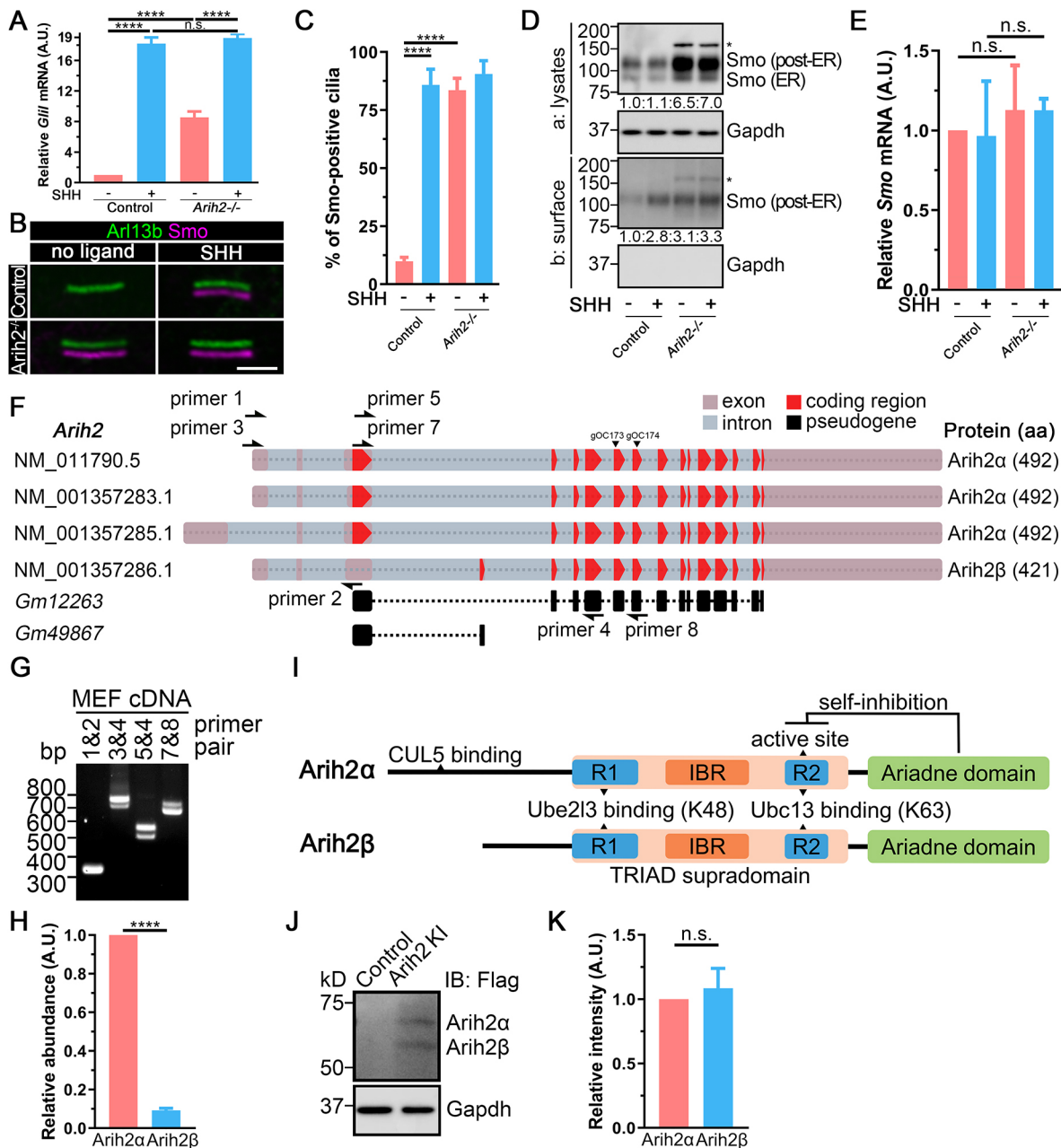


**Fig. 1. Mice express two isoforms of *Arih2*.** (A) qRT-PCR showing the relative endogenous *Gli1* mRNA in control (GreenBomb) and *Arih2*<sup>-/-</sup> cells with or without SHH treatment. Results are mean  $\pm$  s.d.,  $n=4$  repeats. \*\*\*\* $P<0.0001$ ; n.s., not significant (two-way ANOVA with Sidak post-hoc test). (B) Immunofluorescence showing Smo (Flag, magenta) and cilia (Arl13b, green) in control (GreenBomb) and *Arih2*<sup>-/-</sup> cells. Scale bar: 3 μm. Magenta and green channels are offset for presentation. (C) Quantification of Smo-positive cilia described in panel B. Results are mean  $\pm$  s.d.,  $n=6$  repeats with 200 cilia counted per experiment. \*\*\*\* $P<0.0001$  (two-way ANOVA with Sidak post-hoc test). (D) Top (a) is a western blot of whole-cell extracts from control and *Arih2*<sup>-/-</sup> cells with or without SHH treatment to show total Smo levels. The asterisk marks an unspecific band. Gapdh is a loading control. Bottom (b) is a western blot of surface-exposed Smo detected after surface biotinylation and immunoprecipitation. Relative amounts of Smo are listed on the bottom. Blot shown is representative of three repeats. (E) qRT-PCR showing the relative *Smo* mRNA levels in control and *Arih2*<sup>-/-</sup> cells with or without SHH treatment. Results are mean  $\pm$  s.d.,  $n=4$  repeats. n.s., not significant (two-way ANOVA with Sidak post-hoc test). (F) Diagram of the four *Arih2* splice variants that code for either *Arih2* $\alpha$  (492 residues) or *Arih2* $\beta$  (421 residues). *Gm12263* and *Gm49867* are pseudogenes derived from *Arih2*. (G) RT-PCR using primers described in F show that MEFs express splice variants that potentially code for both isoforms. (H) Relative number of reads corresponding to *Arih2* $\alpha$  and *Arih2* $\beta$  by deep sequencing of amplicons with primer set 5&4 against MEF cDNA. Results are mean  $\pm$  s.d.,  $n=4$  repeats. \*\*\*\* $P<0.0001$  by independent two-sample unpaired two-tailed  $t$ -test. (I) Diagram of the domain structure of *Arih2* $\alpha$  and *Arih2* $\beta$ . R1, RING1; IBR, in-between-ring; R2, RING2. R1, IBR and R2 are collectively known as RBR (RING-between-RING-RING) or TRIAD [two RING fingers and a double RING finger linked (DRIL)]. (J) Western blot of cells with a Flag tag knocked into *Arih2* just before the stop codon show that approximately equal amounts of each isoform are expressed in MEFs. (K) Quantification of *Arih2* isoform signal intensity from western blots as in I. Results are mean  $\pm$  s.d.,  $n=5$  repeats. n.s., not significant (independent samples unpaired two-tailed  $t$ -test). A.U., arbitrary units.

SHH-induced Hedgehog signaling (Lv et al., 2021). As previously shown, loss of *Arih2* elevated ciliary Smo levels at the basal state (Fig. 1B,C) and increased total cellular Smo levels as detected by western blotting (Fig. 1Da). Loss of *Arih2* did not affect ciliogenesis (Fig. S1). The excess Smo appeared to be largely in intracellular pools, as the amount exposed to the surface in *Arih2* mutant cells was similar to the amount that was surface exposed in control cells stimulated with SHH (Fig. 1D). *Smo* mRNA levels were similar in control and *Arih2*<sup>-/-</sup> cells, suggesting that the increased Smo results from post-transcriptional mechanisms (Fig. 1E).

### **Arih2 has two isoforms**

NCBI Gene (<https://www.ncbi.nlm.nih.gov/gene>) describes four mouse *Arih2* transcript variants that differ at the N-terminal coding region (Fig. 1F). There are also two *Arih2* pseudogenes in the mouse genome, but these are highly mutated and do not appear to express proteins (Fig. 1F). The four transcripts encode isoforms of 492 and 421 residues, which we named *Arih2* $\alpha$  and *Arih2* $\beta$  (Fig. 1F). mRNA representing both isoforms is readily detected in fibroblasts (Fig. 1G) although *Arih2* $\alpha$  mRNA levels appear to be ~10-fold higher than *Arih2* $\beta$  (Fig. 1H). *Arih2* $\alpha$  and *Arih2* $\beta$  are similar with shared ring, ring between ring, and Ariadne domains, but differ at their N-termini. The N-terminus of *Arih2* $\alpha$  carries a cullin-5-binding site that is missing from *Arih2* $\beta$ , whereas the N-terminus of *Arih2* $\beta$  is predicted to encode a signal peptide with a low probability cleavage site (at the alanine residue in position 19) (Fig. 1I) (Kelsall et al., 2013). Even though *Arih2* $\alpha$  is expressed at higher levels than *Arih2* $\beta$ , measuring the levels of a Flag-Avi-tag knocked into the endogenous *Arih2* gene just prior to the stop codon suggests that both isoforms are present in the cell at approximately equal levels (Fig. 1J,K).

### **Arih2 $\beta$ regulates Smo levels**

To ensure that the phenotype in the *Arih2* mutant cells was due to the loss of *Arih2*, we rescued *Arih2* mutant cells with constructs that express Myc-tagged *Arih2* $\alpha$  or *Arih2* $\beta$ , and Myc-tagged *Arih2* $\alpha$ <sup>C309A</sup> or *Arih2* $\beta$ <sup>C238A</sup> in which the active sites are mutated (Fig. 2A). Interestingly expression of *Arih2* $\beta$  returned ciliary Smo (Fig. 2B,C) and total Smo (Fig. 2D) levels back to normal, whereas expression of *Arih2* $\alpha$  was not effective at doing this. *Arih2* $\beta$ <sup>C238A</sup> was not functional indicating that the E3 ubiquitin ligase activity of *Arih2* $\beta$  is required for rescue (Fig. 2B–D).

To determine whether *Arih2* is capable of ubiquitylating Smo, we transfected HEK293 cells with Smo–Flag and Ty1–ubiquitin along with *Arih1*, *Arih2* $\alpha$ , *Arih2* $\alpha$ <sup>C309A</sup>, *Arih2* $\beta$  or *Arih2* $\beta$ <sup>C238A</sup>. Immunoprecipitating Smo–Flag and measuring the incorporation of Ty1–ubiquitin indicated that cells expressing *Arih2* $\beta$  incorporated more ubiquitin onto Smo than cells expressing the *Arih2* $\beta$  active site mutation or the *Arih2* $\alpha$  and *Arih1* isoforms (Fig. 2H).

To explore physical interactions between Smo and *Arih2*, we used the recently developed fluorescent protein–protein interaction (Fluoppi) approach (Watanabe et al., 2017). In this method, one protein is tagged with an Azami-Green (AG) fluorescent tag and the other protein is tagged with the PB1 homodimerization domain from the p62 autophagy protein (Fig. 2E). If the bait and prey proteins do not interact, the AG fluorescence will reflect the distribution of its fusion partner. If the bait and prey interact, the AG fusion protein will be drawn to the PB1 clusters, and the fluorescence will appear as puncta in the cytoplasm. *Arih2* $\alpha$ –AG expressed alone or co-expressed with Smo–PB1 showed the same localization pattern in the cytoplasm and nucleus indicating no interaction between *Arih2* $\alpha$  and Smo (Fig. 2F). *Arih2* $\beta$ –AG

expressed alone showed cytoplasmic localization, which was redistributed to strong puncta when co-expressed with Smo–PB1, indicating a physical interaction (Fig. 2F). Deletion of the Ariadne domain of *Arih2* $\beta$  or the C-terminal tail of Smo abolished the interaction, whereas the interaction was maintained when the Triad domain was deleted (Fig. 2G).

### **Arih2 $\beta$ localizes to the ER**

Previously, we reported that *Arih2* was localized predominately in the nucleus with a lower amount in the cytoplasm and none detected in the cilium (Lv et al., 2021). However, this work only examined the 492-residue *Arih2* $\alpha$  isoform. Since *Arih2* $\beta$  is relevant to Hedgehog signaling, we repeated this work and examined both isoforms. We could not detect ciliary localization with either isoform (Fig. 3A). As previously shown, *Arih2* $\alpha$  localized predominately to the nucleus with some cytoplasmic localization in mouse embryonic fibroblasts (MEFs) (Fig. 3A,B), which is similar to the distribution of its paralog *Arih1* (Fig. S2A). *Arih2* $\alpha$  in the cytoplasm did not appear to associate with any cytoskeletal or vesicular structures. In contrast to the prominent nuclear localization of *Arih2* $\alpha$ , *Arih2* $\beta$  localizes to the cytoplasm with no localization in the nucleus (Fig. 3A,B). Within the cytoplasm, *Arih2* $\beta$  was concentrated near the nucleus where it associated with tubular and vesicular structures, and colocalized with cell body Smo (Fig. 3B). A similar localization of both isoforms was seen in IMCD3, hTERT RPE-1, HEK 293T and NIH/3T3 cells (Fig. S2B). No association was seen between *Arih2* $\beta$  and endosomes or the Golgi complex (Fig. S2C,D), and the localization of *Arih2* $\beta$  was not affected by brefeldin A (BFA) treatment (Fig. S2D). However, extensive colocalization was observed between *Arih2* $\beta$  and an ER-targeted GFP construct and the ER-localized ubiquitin E3 ligase Syvnl1 (Fig. 3C) (Kaneko et al., 2002).

*Arih2* $\alpha$  and *Arih2* $\beta$  differ at their N-termini. The N-terminus of *Arih2* $\beta$  is critical for localizing it to the ER, as a form with a C-terminal GFP fusion is retained at the ER, whereas that with an N-terminal GFP fusion is dispersed throughout the cell (Fig. 3D). To identify the ER localization signal of *Arih2* $\beta$ , we generated a series of deletions where the N-terminal helical domains were progressively removed starting at the RING1 domain and moving back toward the N-terminus. Immunofluorescence results showed that the first 22 residues, which are evolutionally conserved in mammals, are necessary for the ER localization of *Arih2* $\beta$  (Fig. 3E). Inserting GFP after the 22nd residue did not disrupt ER localization. However, GFP fusions that only carried the first 22 *Arih2* $\beta$  residues are not as highly enriched at the ER, suggesting that other portions of *Arih2* $\beta$  also contribute to ER localization (Fig. 3F). Fluoppi analysis showed that the Ariadne domain is needed for interaction with Smo (Fig. 2G), indicating that Smo binding might enhance ER enrichment of *Arih2* $\beta$ .

### **Arih2 $\beta$ localizes to the cytoplasmic face of the ER**

The signal sequence at the N-terminus of *Arih2* $\beta$  could function to tether *Arih2* $\beta$  to the outer surface of the ER or it could direct the translocation of *Arih2* $\beta$  into the lumen of the ER. There is currently no evidence for ubiquitylation activity in the lumen of the ER, suggesting that the signal sequence is more likely to function to tether the protein to the cytoplasmic surface of the ER. However, to distinguish these possibilities, we made *Arih2* $\beta$  fusions to the Ca<sup>2+</sup>-measuring organelle-entrapped protein indicators (CEPIA) (Suzuki et al., 2014) (Fig. 4A,B). CEPIA is a Ca<sup>2+</sup> indicator that is fluorescent when exposed to high Ca<sup>2+</sup> levels as found in the ER lumen but is non-fluorescent in the lower Ca<sup>2+</sup> environment of the

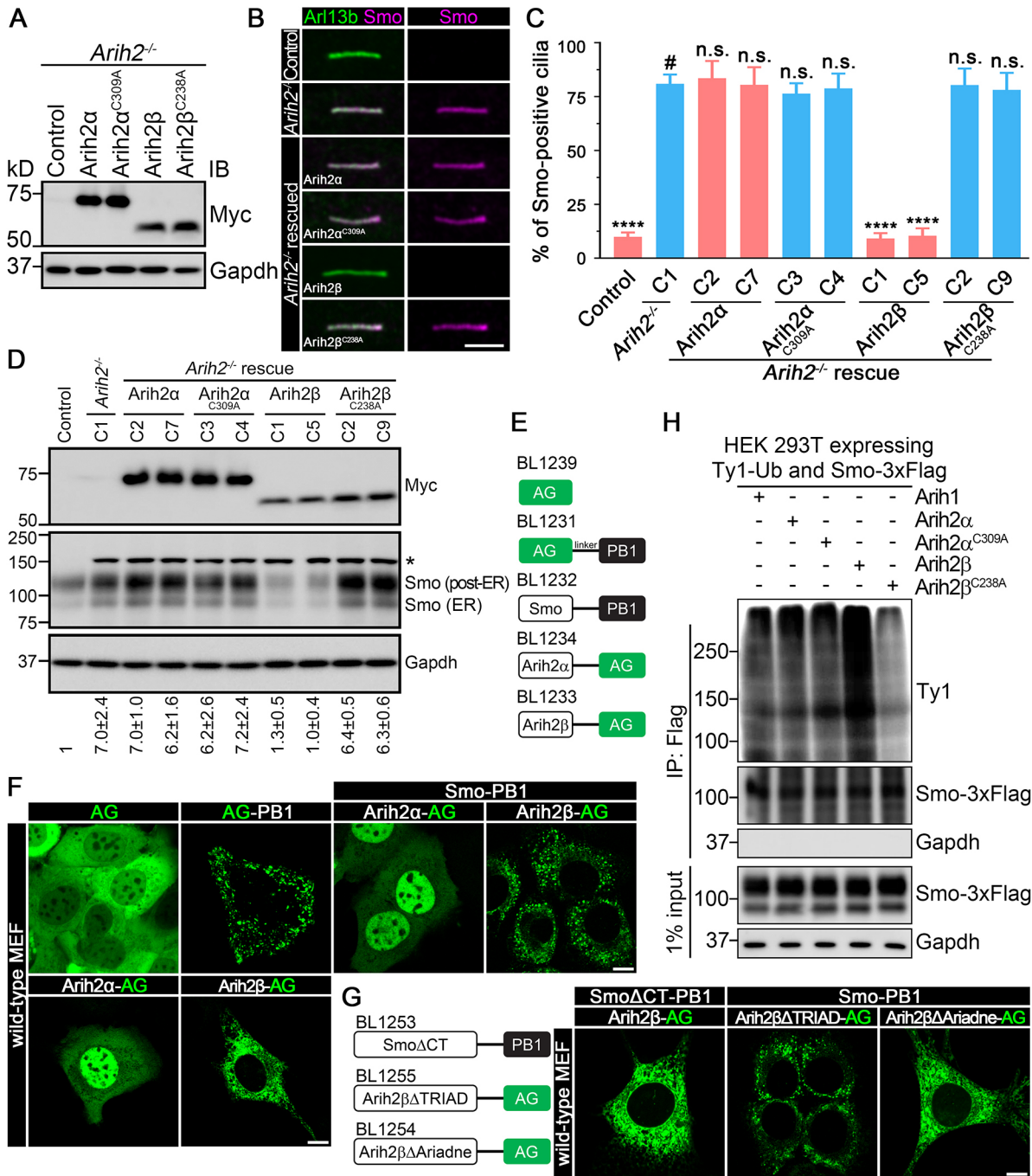


**Fig. 2. Aih2β regulates Smo levels.** (A) Western blot of untransfected *Aih2*<sup>-/-</sup> cells (control) and *Aih2*<sup>-/-</sup> cells rescued with Myc-tagged Aih2α (plasmid BL256) and Aih2β (plasmid BL929) along with the enzymatic dead versions Aih2α<sup>C309A</sup> (plasmid BL368) and Aih2β<sup>C238A</sup> (plasmid BL930). Blot shown is representative of three repeats. (B) Immunofluorescence images showing Smo (Flag, magenta) and cilia (Arl13b, green) in MEF<sup>Smo-3xFlag</sup> (control), *Aih2*<sup>-/-</sup> cells and *Aih2*<sup>-/-</sup> cells rescued with Myc-tagged Aih2α and Aih2β along with the enzymatic dead versions Aih2α<sup>C309A</sup> and Aih2β<sup>C238A</sup>. Scale bar: 3 μm. (C) Quantification of ciliary Smo localization from images as in B. Results are mean±s.d., n=6 repeats with 200 cilia counted per experiment. n.s., not significant, \*\*\*\*P<0.0001 [two-way ANOVA with Tukey post-hoc test compared to *Aih2*<sup>-/-</sup> cells (labeled with #)]. (D) Western blots to quantify rescue of total Smo levels by Myc-tagged Aih2α and Aih2β along with the enzymatic dead versions Aih2α<sup>C309A</sup> and Aih2β<sup>C238A</sup>. Two independent rescue lines are shown for each construct. The amount of total Smo relative to control (GreenBomb) is shown on the bottom. The asterisk marks an unspecific band. Gapdh is a loading control. (E) Diagram of Fluoppi constructs used. The AG domain is an Azami-Green fluorescent reporter and the PB1 domain consists of homodimerization domain from the p62 autophagy protein. Fluorescent puncta appear in the cytoplasm when the two domains are brought together as fusion protein (AG-PB1 is a positive control) or by a protein-protein interaction (Watanabe et al., 2017). (F) Live-cell images of MEF cells expressing each of the constructs described in E. Note that cells expressing Smo-PB1 with Aih2β-AG show cytoplasmic puncta similar to the positive control AG-PB1. Scale bars: 5 μm. (G) Live-cell images of MEF cells expressing Smo deleted of the C-terminal tail (plasmid BL1253) and Aih2β deleted of the TRIAD domain (BL1255) or Ariadne domain (plasmid BL1254). Scale bar: 5 μm. Images shown in F and G are representative of three repeats. (H) Ligation of ubiquitin onto Smo by Aih2. HEK 293T cells expressing Smo-3xFlag (plasmid PD22) and Ty1-ubiquitin (plasmid BL1035) were transiently transfected with the constructs indicated on the top. After lysis, Smo was immunoprecipitated (IP) with Flag resin and examined by western blotting with antibodies listed on the right side. Input are extracts before Flag immunoprecipitation (1%). Blots shown are representative of three repeats.

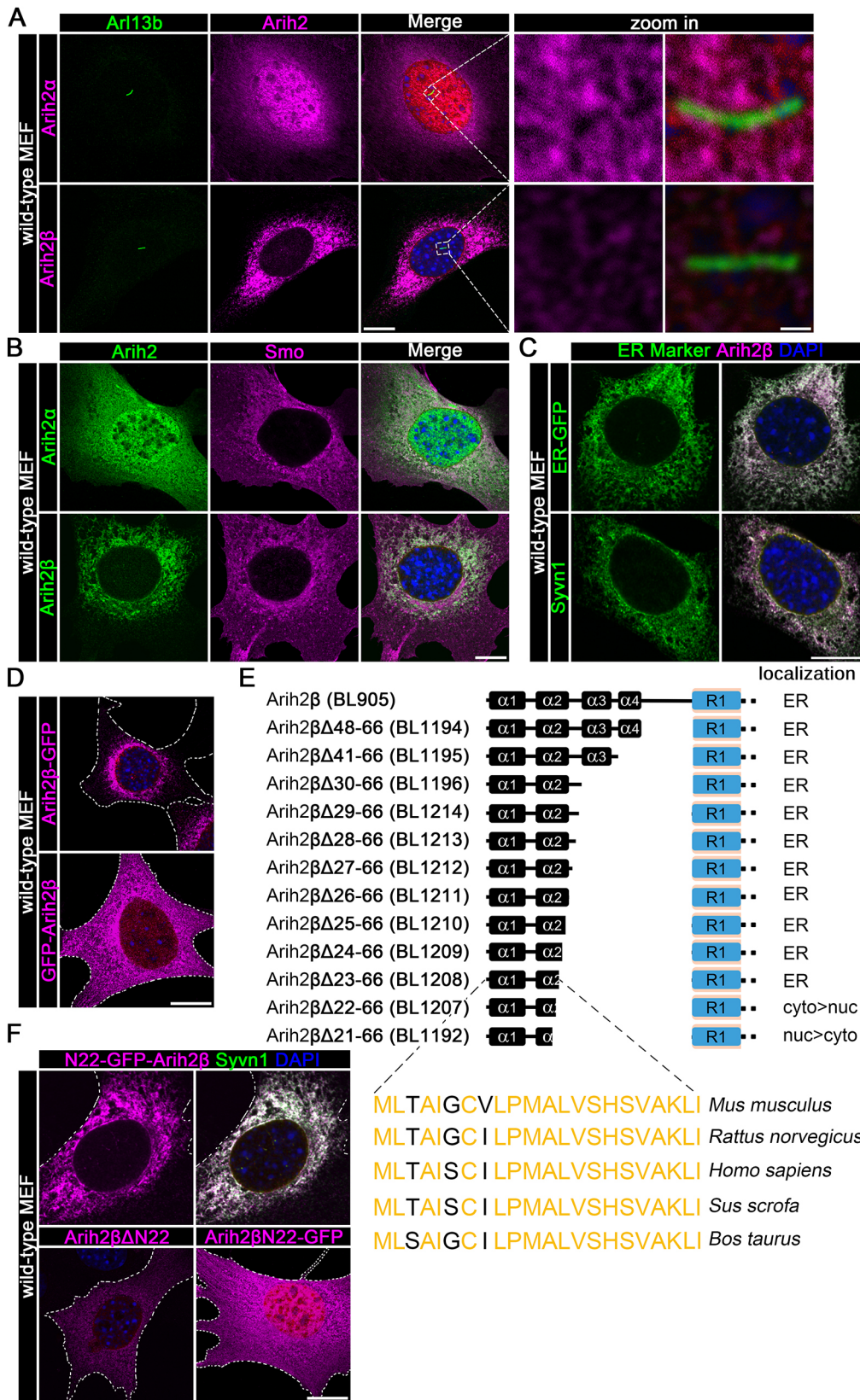


**Fig. 3. Arih2 $\beta$  localizes to the ER.** (A) Wild-type MEF cells expressing Flag-tagged Arih2 $\alpha$  (plasmid BL225) and Arih2 $\beta$  (plasmid BL905) were stained for Arih2 (Flag, magenta), cilia (Arl13b, green), and DNA (DAPI, blue). Scale bars: 5  $\mu$ m (main images); 1  $\mu$ m (enlarged images). (B) Wild-type MEF cells expressing Flag-tagged Arih2 $\alpha$  (plasmid BL225) and Arih2 $\beta$  (plasmid BL905) were stained for Arih2 (Flag, green), Smo (magenta), and DNA (DAPI, blue). Scale bar: 5  $\mu$ m. (C) Wild-type MEF cells expressing Flag-tagged Arih2 $\beta$  and the ER markers ER-GFP (plasmid BL1099) or Synv1-HA (plasmid BL1087) were stained for Arih2 (Flag, magenta), the ER marker (GFP or HA, green), and DNA (DAPI, blue). Scale bar: 5  $\mu$ m. (D) Wild-type MEF cells expressing Arih2 $\beta$ -GFP (BL1117) and GFP-Arih2 $\beta$  (BL1118). Cell outlines are shown by dotted lines. Scale bar: 5  $\mu$ m. (E) Diagram of the N-terminus of Arih2 $\beta$  with a series of truncations produced to test the possible ER signal peptide. The four  $\alpha$ -helices were predicted by PSIPRED 4.0. (F) Wild-type MEF cells expressing Arih2 $\beta$  with GFP inserted after residue 22 (N22-GFP-Arih2 $\beta$ , plasmid BL1218, magenta) and Synv1-HA (BL1087, green). Bottom row: wild-type MEF cells expressing Arih2 $\beta$  missing the first 22 residues (Arih2 $\beta$  $\Delta$ N22, BL1217, magenta) and the first 22 residues of Arih2 $\beta$  fused to GFP (Arih2 $\beta$ N22-GFP, BL1219, magenta). Scale bar: 5  $\mu$ m. Images shown in A–D and F are representative of three repeats.

cytoplasm (Fig. 4C). Targeting CEPIA to the ER lumen by fusion with a modified ER signal sequence from the mouse immunoglobulin heavy chain variable region yielded a high fluorescent signal. However, fusion of CEPIA to C-terminus of Arih2 $\beta$  or inserting it after the signal sequence at the N-terminus

correctly localized the indicator to the ER but produced little signal (Fig. 4C). The lack of signal indicates that the CEPIA domain in these constructs is in the cytoplasm supporting a model where the signal sequence of Arih2 $\beta$  tethers the protein onto the cytoplasmic face of the ER.

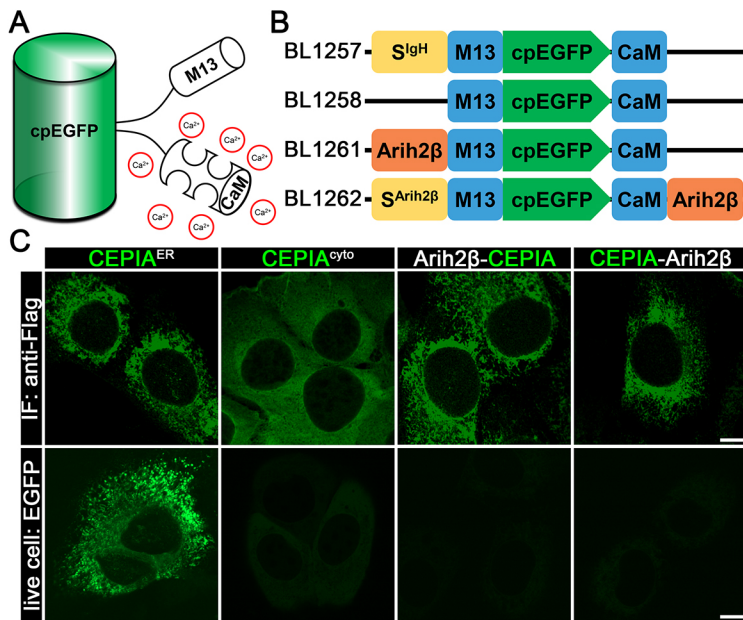


**Fig. 4. Arih2 $\beta$  localizes in the cytoplasmic side of the ER.**

(A) Diagram of the CEPIA Ca<sup>2+</sup> indicator, which is a circularly permuted EGFP (cpEGFP) flanked by the myosin light chain M13 helix and calmodulin (CaM). (B) Diagram of constructs used. S<sup>Arih2 $\beta$</sup>  is the first 22 residues of Arih2 $\beta$ . (C) MEFs expressing each of the constructs in B was stained for Flag (top row) or imaged live for CEPIA fluorescence (bottom row). Scale bar: 5  $\mu$ m. Images shown are representative of three repeats.

### Arih2 loss promotes ER stress

Prior to our finding that Arih2 $\beta$  localizes to the ER, more than 30 E3 ligases had been localized to this organelle where they are thought to function primarily in protein quality control, but they also regulate Ca<sup>2+</sup> release and cholesterol biosynthesis (Rusilowicz-Jones et al., 2021). Our finding that cellular Smo levels are increased by the loss of Arih2 suggests that this E3 is regulating the destruction of excess or misfolded Smo. Transmembrane proteins in the ER typically undergo proteasomal degradation via ER-associated degradation (ERAD). During ERAD, cytoplasmic domains of misfolded membrane proteins become ubiquitylated, targeting them for extraction from the membrane by Vcp (also known as p97 and Cdc48) and degradation by the proteasome (Bodnar and Rapoport, 2017). Treatment of control cells with eeyarestatin I (EerI), which blocks ERAD by inhibiting Vcp (Wang et al., 2008), elevated levels of the ER form of Smo and promoted the production of high molecular mass forms of Smo (Fig. 5A; Fig. S3). These higher molecular mass forms are not seen in the parental cell line, indicating that they are not simply a cross reactive product (Fig. S4). It is likely that these larger forms are polyubiquitylated Smo forms, which under normal conditions would be degraded by ERAD but accumulate when ERAD is blocked. If Arih2 is responsible for targeting misfolded Smo for degradation, we would expect that the amount of ubiquitylated Smo that accumulates upon EerI treatment would be reduced in *Arih2* mutants. Supporting this idea, blocking ERAD with EerI without blocking translation caused a greater accumulation of ubiquitylated Smo in control cells compared to in *Arih2* mutant cells (Fig. 5A–C).

The ER accumulation of Smo and other potential Arih2 $\beta$  substrates in *Arih2* mutants is likely to cause ER stress and the unfolded protein response. Consistent with this idea, protein aggregates as detected with thioflavin T (Beriault and Werstuck, 2013) were as abundant in untreated *Arih2* mutant cells as they are in control cells treated with the ERAD inhibitor EerI (Fig. 5D). As a more direct test, we measured expression of unfolded protein response target genes (Osowski and Urano, 2011). Changes were consistent with an increased unfolded protein response, with *Atf4*, *Hspa5*, *Ddit3*, *Hsp90b1* and spliced *Xbp1* increased, and unspliced *Xbp1* decreased in *Arih2* mutant cells (Fig. 5E).

### DISCUSSION

Our findings show that Arih2 loss elevates basal expression of Hedgehog-responsive genes, increases the total cellular level of Smo and causes Smo to accumulate in cilia at the basal state. Arih2, also known as Triad1, is a ring-between-ring E3 ligase that functions with the E2 conjugating enzyme Ube213 to ubiquitylate substrates. Consistent with Ube213 being a functional E2 for Arih2, we found that Ube213 loss also elevated cellular levels of Smo (Lv et al., 2021). In mouse, Arih2 encodes two major isoforms that differ at their N-termini. Arih2 $\alpha$  has a longer N-terminus that includes a cullin-5-binding site and localizes to the nucleus, whereas the N-terminus of Arih2 $\beta$  has a hydrophobic helix that anchors it to the cytoplasmic face of the ER. Expression of the ER-localized Arih2 $\beta$  isoform fully rescues the Smo phenotypes caused by loss of Arih2, whereas the nuclear-localized form does not. Most work on Arih2 focuses on the role of Arih2 $\alpha$  as part of the cullin-5 complex (Hüttenhain et al., 2019; Kelsall et al., 2013; Kosthron et al., 2021). Complete loss of Arih2 in mouse leads to embryonic lethality and increased inflammatory responses (Lin et al., 2013). Heterozygotes show a variety of structural birth defects in kidney, skin, bone, and heart (<https://www.mousephenotype.org/data/genes/MGI:1344361>; Bult et al., 2019; Dickinson et al., 2016), which are similar to phenotypes caused by cilia dysfunction.

The localization of Arih2 $\beta$  at the ER and our finding that loss of Arih2 elevates total Smo levels suggest that Arih2 regulates the production of Smo, possibly through a quality control mechanism (Fig. 5F). Misfolded proteins in the ER are targeted for degradation by the ERAD system. During ERAD, misfolded proteins are targeted to a dislocation complex in the ER membrane where the misfolded protein is polyubiquitylated on cytoplasmic lysine residues. The polyubiquitylated protein is removed from the membrane by the Vcp complex and sent to the proteasome for degradation. The major E3 ligases involved in ERAD are thought to be Syn1 and Amfr. However, more than a dozen other E3s have been implicated in ERAD of specific substrates (Olzmann et al., 2013), and more than 30 E3s localize to the ER (Fenech et al., 2020; Rusilowicz-Jones et al., 2021). Our finding that loss of Arih2 reduces the incorporation of ubiquitin onto Smo when ERAD is blocked by the Vcp inhibitor EerI supports a

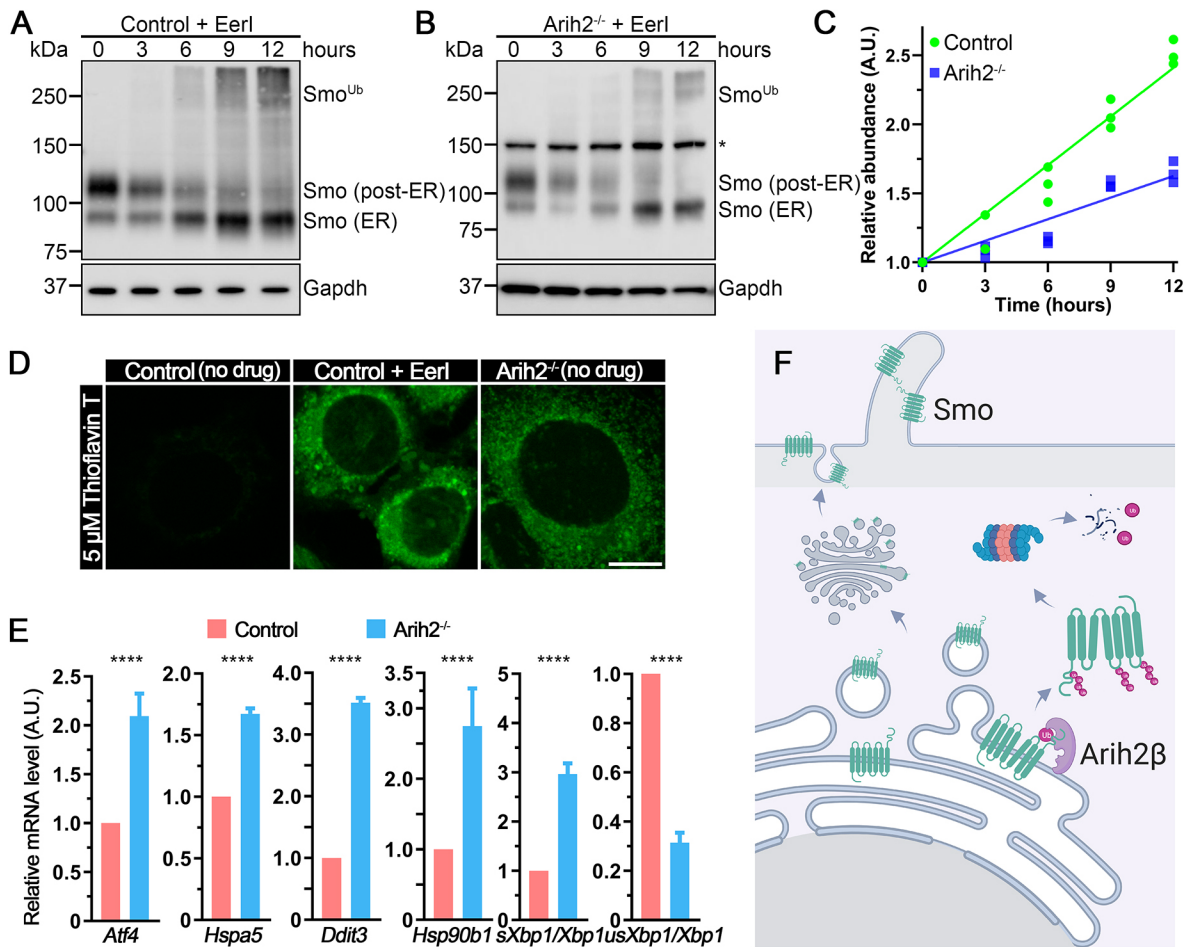


**Fig. 5. Aih2 $\beta$  mediates Smo ubiquitylation and ERAD.** (A,B) Control (A) and *Aih2*<sup>-/-</sup> (B) cells were treated with Eerl but not cycloheximide. Cells were collected at 0, 4, 8 and 12 h and analyzed by anti-Flag western blotting. Note that exposure times for the two blots were chosen to approximately equalize intensity of Smo at the 0 time point. The asterisk marks a nonspecific band. Gapdh is a loading control. (C) Quantification of the level of ubiquitylated forms of Smo (signal above \* at 150 kD) from blots as in A,B.  $n=3$ . Linear curve fitting is used here. The slopes of linear regression equations established differ significantly ( $P<0.001$ ). (D) Thioflavin T fluorescence staining of aggregated proteins in control, control treated with Eerl, and *Aih2*<sup>-/-</sup> cells. Scale bar: 5  $\mu$ m. Images shown are representative of three repeats. (E) qRT-PCR showing the relative endogenous *Atf4*, *Hspa5*, *Ddit3*, *Hsp90b1*, spliced *Xbp1* relative to overall *Xbp1* (*sXbp1/Xbp1*), and unspliced *Xbp1* relative to overall *Xbp1* (*usXbp1/Xbp1*) mRNA in control (GreenBomb) and *Aih2*<sup>-/-</sup> cells. Results are mean $\pm$ s.d.,  $n=3$  repeats. \*\*\*\* $P<0.0001$  (independent samples unpaired two-tailed *t*-test). (F) Model for the function of Aih2 in regulating Smo levels in the cell. ER-localized Aih2 $\beta$  recognizes misfolded or excess Smo and ubiquitylates cytoplasmic lysine residues. The ubiquitylated Smo is extracted from the membrane and sent to the proteasome for degradation. Normally folded Smo exits the ER and traverses the Golgi complex before delivery to the plasma membrane and cilium.

role for Aih2 $\beta$  in ERAD. However, Aih2 is thought to catalyze only the initial mono-ubiquitylation (Hüttenhain et al., 2019; Kelsall et al., 2013), indicating that additional E3 ligases are needed to extend the chain. Syvn1 is an interesting possibility as its loss also elevates expression of Hedgehog-responsive genes, but we did not observe increased ciliary Smo levels in the knockouts (Lv et al., 2021).

The loss of Aih2 elevates the total level of Smo in the cell. The majority of the extra Smo is not exposed on the cell surface. However, exposed Smo is increased in the mutant to about the level seen in activated control cells. Smo is thought to constantly diffuse into cilia with regulated removal dictating the ciliary level (Milenkovic et al., 2009). Increased plasma membrane Smo would increase the amount that diffuses into the cilium. Overexpression of Smo is sufficient to saturate the retrieval process (Corbit et al., 2005), and so it is likely that this is the reason for elevated ciliary Smo in Aih2 mutants. However, ciliary localization of Smo is not sufficient to activate the pathway, raising the question of why the

loss of Aih2 elevates basal expression of Hedgehog responsive genes. It is likely that Aih2 is involved in the production of Smo and is not directly involved in the Hedgehog signal transduction cascade. Activation of Smo is driven by phosphorylation and sterol binding (Deshpande et al., 2019; Jia et al., 2004; Nedelcu et al., 2013; Zhang et al., 2004) but point mutations, such as the SmoM2 W539L mutation, activate the pathway independent of upstream signals. This mutation is thought to shift helices changing the protein into an active conformation (Huang et al., 2018). It is possible that some misfolded protein that escapes the ER in the absence of Aih2 is in an active conformation analogous to the SmoM2 state. Another possibility is that if the loss of Aih2 causes Smo to remain in the ER for an extended time, the high Ca<sup>2+</sup> environment of the ER lumen might promote the esterification of Smo with cholesterol and drive it towards an active conformation (Hu et al., 2022).

In summary, our work identifies a new regulatory mechanism in the ER that controls the cellular levels of Smo. When this

mechanism is defective, ciliary Smo levels are elevated and basal expression through the pathway is increased.

## MATERIALS AND METHODS

### Plasmids

Plasmids were assembled by TEDA method (Xia et al., 2019) into the pHAGE lentiviral backbone (Wilson et al., 2008). All inserts are derived from mouse unless otherwise stated. Mutations were generated by PCR amplification with mutated primers and the corresponding amplicons were TEDA assembled. All inserts were fully sequenced and matched the Ensembl reference sequence, NCBI reference sequence or expected mutant forms. Plasmids are listed in Table S1 and SnapGene files will be provided upon request.

### Cell culture

Wild-type mouse embryonic fibroblasts (MEFs) were derived from E14 embryos and immortalized with SV40 Large T antigen. These cells were cultured in 95% DMEM (4.5 g/l glucose), 5% fetal bovine serum (FBS), 100 U/ml penicillin, and 100 µg/ml streptomycin. IMCD3 cells (obtained from Jagesh Shah, Harvard Medical School, Boston, USA) were cultured in 42.5% DMEM (4.5 g/l glucose), 42.5% F12, 5% FBS, 100 U/ml penicillin and 100 µg/ml streptomycin. NIH/3T3 cells (obtained from Stephen Doxsey, UMass Medical School, Worcester, USA) and HEK 293T cells (obtained from Julie Jonassen, UMass Medical School, Worcester, USA) were cultured in 90% DMEM (4.5 g/l glucose), 10% FBS, 100 U/ml penicillin and 100 µg/ml streptomycin. hTert RPE-1 cells (obtained from Stephen Doxsey) were cultured in 90% DMEM (1 g/l glucose), 10% FBS, 100 U/ml penicillin and 100 µg/ml streptomycin (all from Gibco-Invitrogen). Cells were confirmed to be of mouse or human origin as expected and monitored for mycoplasma contamination by PCR (Tang et al., 2000) and DAPI staining.

For smoothed agonist (SAG) experiments, MEFs were plated at near-confluent densities and serum starved (same culture medium described above but with 0.25% FBS) for 24 h prior to treatment to allow ciliation. SAG (Calbiochem) was used at 400 nM.

Sonic hedgehog (SHH) conditioned medium was generated from HEK 293T cells expressing plasmids encoding HsSHH (BL243; Table S1), XtScube2 (BL244; Table S1) and MmDisp1 (BL323; Table S1). Cells stably secreting SHH were grown to confluency in 90% DMEM (4.5 g/l glucose), 10% FBS, 100 U/ml penicillin and 100 µg/ml streptomycin; the medium was then replaced with low-serum medium (0.25% FBS) and cells were cultured for a further 24 h. Medium was collected, filtered sterilized with 0.45 µm filter (Millipore) and titered for the ability to cause relocation of Smo to cilia. Dilutions similar in effect to 400 nM SAG were used for experiments.

The chemicals used in this study include protein transport from the ER to the Golgi complex inhibitor brefeldin A (BFA) (50 µg/ml), protein synthesis inhibitor cycloheximide (CHX) (150 µg/ml), the ERAD inhibitor eeyarestatin I (EerI) (50 µM), and the proteasomal degradation inhibitor MG132 (1 µM).

### Lentivirus production

Lentiviral packaged pHAGE-derived plasmids (Wilson et al., 2008) were used for transfection. These vectors are packaged by a third-generation system comprising four distinct packaging vectors (Tat, Rev, Gag/Pol, VSV-g or MLV-env) using HEK 293T cells as the host. DNA (plasmid of interest, 5 µg; Tat, 0.5 µg; Rev, 0.5 µg; Gag/Pol, 0.5 µg; VSV-g/MLV-env, 1 µg) was delivered to the HEK 293T cells as calcium phosphate precipitates. After 48 h, the supernatant was harvested, filtered through a 0.45 µm filter (Millipore), and added to subconfluent cells. After 24 h, cells were selected with corresponding antibiotics [nourseothricin (Nat, 50 µg/ml), puromycin (Puro, 1 µg/ml), zeocin (Zeo, 500 µg/ml) or blasticidin (Bsd, 60 µg/ml)].

### Flow cytometry

For flow sorting, pelleted cells (2000 g for 3 min) were resuspended in the corresponding media and sorted into tubes or 96-well plates containing medium with 10% fetal bovine serum by a BD FACS C-Aria II Cell Sorter (BSL-2+/BSC).

### Genome editing

Guide RNAs were selected from the Brie library (Doench et al., 2016) or designed using CHOPCHOP (Labun et al., 2019). Corresponding oligonucleotides were cloned into lentiCRISPR v2 Puro (Addgene plasmid #52961, deposited by Feng Zhang; Sanjana et al., 2014) or lentiCRISPR v2 Puro<sup>P93S</sup> (BL245) and screened by sequencing. lentiCRISPR v2 Puro<sup>P93S</sup> is like its parent except for a proline to serine mutation in the puromycin N-acetyl-transferase gene, which increases its resistance to Puro (<https://www.addgene.org>). The vectors were packaged into lentiviral particles and transfected into MEF cells. After selection, the pools were analyzed by flow cytometry. Individual cells were sorted into 96-well plates by flow cytometry or dilution cloning. Single mutant clones were identified with Sanger sequencing, GENEWIZ Amplicon-EZ sequencing, immunofluorescence or immunoblotting. Sequencing results were analyzed with GEAR Indigo (<https://www.gear-genomics.com>), Poly peak parser and the SWS method (Hill et al., 2014; Jie et al., 2017; Rausch et al., 2020).

Flag-Avi knock-in was achieved by using CRISPR-Cas9 genome editing. Cas9 and sgRNA were expressed from lentiCRISPR v2 Puro (BL1139; Table S1). The template for homology-directed repair was designed in Benchling (<https://www.benchling.com/>). Each homology arm was about 600 bp. The main components of the donor sequence are left arm-3xFlag-Avi (containing a stop codon)-loxP-IRES2-Puro-loxP-right arm. The donor (BL1137; Table S1) and guide RNA vectors (BL1139) were transfected into cells with Qiagen Effectene Transfection Reagent according to the manufacturer's protocol. Transfected cells were drug-selected with Puro and then tested in population.

### Next generation sequencing and data analyzing

PCR products were analyzed by Amplicon-EZ paired-end sequencing (Azenta Genewiz). Using bwa-mem2 (<https://github.com/bwa-mem2>) with default parameters, paired-end sequencing reads from each replicate were first aligned to *Arih2* pseudogenes (Gm12263 and Gm49867), which contain many substitutions compared to the parental *Arih2* gene; unmapped reads were then extracted and mapped onto the enriched region of *Arih2*. Because the cassette exon is specifically spliced out in *Arih2β* but not *Arih2α*, sequencing read pairs were deemed to belong to *Arih2β* if they cover the cassette exon with an overhang of at least 5 nucleotides, otherwise they were considered as reads from *Arih2α*.

### Immunofluorescence and live-cell imaging

Cells were fixed with 2% paraformaldehyde for 15 min, permeabilized with 0.1% Triton-X-100 for 2 min and stained as described previously (Follit et al., 2006). In some cases, fixed cells were treated with 0.05% SDS for 5 min before prehybridization to retrieve antigens. The primary and secondary antibodies are described in Table S2. For the thioflavin T fluorescence assay, cells were incubated with 5 µM thioflavin T (Millipore Sigma) for 10 min before fixation (Beriault and Werstuck, 2013).

For live-cell imaging, cells were seeded in 35 mm glass bottom collagen-coated dishes (MatTek Corporation) and cultured for at least 24 h before imaging.

Confocal images were taken with a LSM910 equipped with a 63× objective and converted into a maximum projection with ZEN 3.1 blue edition (Zeiss).

### Protein and mRNA analysis

For western blots, cells were pelleted (2000 g for 3 min) and lysed directly with denaturing gel loading buffer [Tris-HCl 125 mM pH 6.8, 20% (v/v) glycerol, 4% (v/v) SDS, 10% (v/v) β-mercaptoethanol, and 0.04% Bromophenol Blue]. The primary and secondary antibodies are described in Table S2. Western blots were developed by chemiluminescence (Super Signal West Dura, Pierce Thermo) and imaged using an Amersham Imager 600 imager (GE Healthcare Life Sciences). Bands were quantified with Gel-Pro Analyzer 4 (Meyer Instruments).

For immunoprecipitations, cells were serum starved for 48 h and proteins were extracted with lysis buffer (20 mM HEPES pH 7.5, 50 mM KCl, 1 mM MgCl<sub>2</sub>) with 0.5% digitonin and protease inhibitor (cOmplete EDTA-Free, Roche). Insoluble components were removed by centrifugation at 20,000 g. Primary antibodies pre-adsorbed to protein G-Sepharose beads (GE



Healthcare) were added to the cell extract and the mixture incubated for 2 h at 4°C. After centrifugation (200 g for 1 min), beads were washed with lysis buffer supplemented with 0.1% digitonin before elution in denaturing gel loading buffer for SDS-PAGE electrophoresis and western blotting analysis.

Isolation of mRNA and quantitative mRNA analysis was performed as previously described (Jonassen et al., 2008) using the primers tabulated in Table S3.

### Biotinylation of cell surface proteins

Cell surface proteins were biotinylated by a non-cell permeable EZ-Link Sulfo-NHS-SS-Biotin (Thermo Fisher Scientific) as described previously (Pusapati et al., 2018). Cells with surface proteins biotinylated were lysed with CelLytic M solution containing cOComplete, EDTA-free Protease Inhibitor Cocktail (Millipore Sigma). The lysate was clarified by centrifugation at 4°C, 18,000 g for 10 min. Biotinylated proteins were captured and purified from the supernatant by Pierce High Capacity NeutrAvidin agarose (Thermo Fisher Scientific). After washing six times with lysis buffer, the beads were extracted with denaturing gel loading buffer containing 100 mM DTT at 37°C for 1 h to release biotinylated proteins.

### Ubiquitylation assay

The Smo ubiquitylation assay was performed as described previously (Lv et al., 2021). In brief, HEK 293T cells were plated at 60% confluent density onto a 10 cm plate. After 24 h, the cells were transfected with 5 µg of each vector using calcium phosphate transfection. At 24 h after transfection, cells were treated with 50 µM Eeyarestatin I and 1 µM MG132 for 4 h to block ERAD and proteasomal degradation. Cells were lysed and Smo was captured with anti-Flag M2 affinity gel (Millipore Sigma) as described in the immunoprecipitation method in Protein and mRNA analysis section.

### Statistical analysis

Statistical results were obtained from at least three independent experiments. Statistical differences between groups were tested by one-way ANOVA, two-way ANOVA, or repeated measures ANOVA with Sidak or Tukey post-hoc tests in GraphPad Prism 7.04. Differences between groups were considered statistically significant if  $P < 0.05$ . Otherwise, results were labeled as non-significant (n.s.). Statistical significance is denoted with asterisks ( $*P < 0.05$ ;  $**P < 0.01$ ;  $***P < 0.001$ ,  $****P < 0.0001$ ). Error bars indicate standard deviation (s.d.).

### Acknowledgements

We thank Dr Carol E. Schrader and the staff of the University of Massachusetts Medical School Flow Cytometry Core for assistance during this project. Flow Cytometry Resources were supported by National Institutes of Health S10 1S10OD028576 to Carol E. Schrader. We thank Drs Vadim Arshavsky and William Spencer (Duke University) for comments on this work.

### Competing interests

The authors declare no competing or financial interests.

### Author contributions

Conceptualization: B.L., G.J.P.; Methodology: B.L., X.-O.Z., G.J.P.; Validation: B.L., G.J.P.; Formal analysis: B.L., X.-O.Z., G.J.P.; Investigation: B.L., G.J.P.; Writing - original draft: B.L., G.J.P.; Writing - review & editing: B.L., X.-O.Z., G.J.P.; Visualization: B.L.; Supervision: G.J.P.; Funding acquisition: G.J.P.

### Funding

This work was supported by the National Institutes of Health (GM060992 to G.J.P.). Deposited in PMC for release after 12 months.

### Peer review history

The peer review history is available online at <https://journals.biologists.com/jcs/lookup/doi/10.1242/jcs.260299>.reviewer-comments.pdf.

### References

Aguilera, M., Oliveros, M., Martínez-Padrón, M., Barbas, J. A. and Ferrús, A. (2000). Ariadne-1: a vital Drosophila gene is required in development and defines a new conserved family of ring-finger proteins. *Genetics* **155**, 1231-1244. doi:10.1093/genetics/155.3.1231

Beriault, D. R. and Werstuck, G. H. (2013). Detection and quantification of endoplasmic reticulum stress in living cells using the fluorescent compound, Thioflavin T. *Biochim. Biophys. Acta* **1833**, 2293-2301. doi:10.1016/j.bbamer.2013.05.020

Bodnar, N. O. and Rapoport, T. A. (2017). Molecular mechanism of substrate processing by the Cdc48 ATPase complex. *Cell* **169**, 722-735.e9. doi:10.1016/j.cell.2017.04.020

Bult, C. J., Blake, J. A., Smith, C. L., Kadin, J. A. and Richardson, J. E. (2019). Mouse genome database (MGD) 2019. *Nucleic Acids Res.* **47**, D801-d806. doi:10.1093/nar/gky1056

Corbit, K. C., Aanstad, P., Singla, V., Norman, A. R., Stainier, D. Y. and Reiter, J. F. (2005). Vertebrate Smoothed functions at the primary cilium. *Nature* **437**, 1018-1021. doi:10.1038/nature04117

Desai, P. B., Stuck, M. W., Lv, B. and Pazour, G. J. (2020). Ubiquitin links smoothed to intraflagellar transport to regulate Hedgehog signaling. *J. Cell Biol.* **219**, e201912104. doi:10.1083/jcb.201912104

Deshpande, I., Liang, J., Hedeon, D., Roberts, K. J., Zhang, Y., Ha, B., Latorraca, N. R., Faust, B., Dror, R. O., Beachy, P. A. et al. (2019). Smoothed stimulation by membrane sterols drives Hedgehog pathway activity. *Nature* **571**, 284-288. doi:10.1038/s41586-019-1355-4

Dickinson, M. E., Flenniken, A. M., Ji, X., Teboul, L., Wong, M. D., White, J. K., Meehan, T. F., Weninger, W. J., Westerberg, H., Adissu, H. et al. (2016). High-throughput discovery of novel developmental phenotypes. *Nature* **537**, 508-514. doi:10.1038/nature19356

Doench, J. G., Fusi, N., Sullender, M., Hegde, M., Vaimberg, E. W., Donovan, K. F., Smith, I., Tothova, Z., Wilen, C., Orchard, R. et al. (2016). Optimized sgRNA design to maximize activity and minimize off-target effects of CRISPR-Cas9. *Nat. Biotechnol.* **34**, 184. doi:10.1038/nbt.3437

Fenech, E. J., Lari, F., Charles, P. D., Fischer, R., Laëtitiya-Thézénas, M., Bagola, K., Paton, A. W., Paton, J. C., Gyrd-Hansen, M., Kessler, B. M. et al. (2020). Interaction mapping of endoplasmic reticulum ubiquitin ligases identifies modulators of innate immune signalling. *eLife* **9**, e57306. doi:10.7554/eLife.57306

Follit, J. A., Tuft, R. A., Fogarty, K. E. and Pazour, G. J. (2006). The intraflagellar transport protein IFT20 is associated with the Golgi complex and is required for cilia assembly. *Mol. Biol. Cell.* **17**, 3781-3792. doi:10.1091/mbc.e06-02-0133

Hill, J. T., Demarest, B. L., Bisgrove, B. W., Su, Y. C., Smith, M. and Yost, H. J. (2014). Poly peak parser: Method and software for identification of unknown indels using sanger sequencing of polymerase chain reaction products. *Dev. Dyn.* **243**, 1632-1636. doi:10.1002/dvdy.24183

Hu, A., Zhang, J. Z., Wang, J., Li, C. C., Yuan, M., Deng, G., Lin, Z. C., Qiu, Z. P., Liu, H. Y., Wang, X. W. et al. (2022). Cholesterolylation of Smoothed is a calcium-accelerated autoreaction involving an intramolecular ester intermediate. *Cell Res.* **32**, 288-301. doi:10.1038/s41422-022-00622-0

Huang, P., Zheng, S., Wierbowski, B. M., Kim, Y., Nedelcu, D., Aravena, L., Liu, J., Kruse, A. C. and Salic, A. (2018). Structural basis of smoothed activation in hedgehog signaling. *Cell* **174**, 312-324.e16. doi:10.1016/j.cell.2018.04.029

Hüttenhain, R., Xu, J., Burton, L. A., Gordon, D. E., Hultquist, J. F., Johnson, J. R., Satkamp, L., Hiatt, J., Rhee, D. Y., Baek, K. et al. (2019). ARIH2 is a Vif-dependent regulator of CUL5-mediated APOBEC3G degradation in HIV infection. *Cell Host Microbe* **26**, 86-99.e7. doi:10.1016/j.chom.2019.05.008

Jia, J., Tong, C., Wang, B., Luo, L. and Jiang, J. (2004). Hedgehog signalling activity of Smoothed requires phosphorylation by protein kinase A and casein kinase I. *Nature* **432**, 1045-1050. doi:10.1038/nature03179

Jie, H., Li, Z., Wang, P., Zhao, L., Zhang, Q., Yao, X., Song, X., Zhao, Y. and Yao, S. (2017). A simple method based on Sanger sequencing and MS Word wildcard searching to identify Cas9-induced frameshift mutations. *Lab. Invest.* **97**, 1500. doi:10.1038/labinvest.2017.83

Jonassen, J. A., San Agustin, J., Follit, J. A. and Pazour, G. J. (2008). Deletion of IFT20 in the mouse kidney causes misorientation of the mitotic spindle and cystic kidney disease. *J. Cell Biol.* **183**, 377-384. doi:10.1083/jcb.200808137

Kaneko, M., Ishiguro, M., Niinuma, Y., Uesugi, M. and Nomura, Y. (2002). Human HRD1 protects against ER stress-induced apoptosis through ER-associated degradation. *FEBS Lett.* **532**, 147-152. doi:10.1016/S0014-5793(02)03660-8

Kelsall, I. R., Duda, D. M., Olszewski, J. L., Hofmann, K., Knebel, A., Langevin, F., Wood, N., Wightman, M., Schulman, B. A. and Alpi, A. F. (2013). TRIAD1 and HHARI bind to and are activated by distinct neddylated Cullin-RING ligase complexes. *EMBO J.* **32**, 2848-2860. doi:10.1038/emboj.2013.209

Kostrhon, S., Prabu, J. R., Baek, K., Horn-Ghetko, D., von Gronau, S., Klügel, M., Basquin, J., Alpi, A. F. and Schulman, B. A. (2021). CUL5-ARIH2 E3-E3 ubiquitin ligase structure reveals cullin-specific NEDD8 activation. *Nat. Chem. Biol.* **17**, 1075-1083. doi:10.1038/s41589-021-00858-8

Labun, K., Montague, T. G., Krause, M., Torres Cleuren, Y. N., Tjeldnes, H. and Valen, E. (2019). CHOPCHOP v3: expanding the CRISPR web toolbox beyond genome editing. *Nucleic Acids Res.* **47**, W171-W174. doi:10.1093/nar/gkz365

Lee, J., Platt, K. A., Censullo, P. and Ruiz i Altaba, A. (1997). Gli1 is a target of Sonic hedgehog that induces ventral neural tube development. *Development* **124**, 2537-2552. doi:10.1242/dev.124.13.2537

- Lin, A. E., Ebert, G., Ow, Y., Preston, S. P., Toe, J. G., Cooney, J. P., Scott, H. W., Sasaki, M., Saibil, S. D., Dissanayake, D. et al. (2013). ARIH2 is essential for embryogenesis, and its hematopoietic deficiency causes lethal activation of the immune system. *Nat. Immunol.* **14**, 27-33. doi:10.1038/ni.2478
- Lv, B., Stuck, M. W., Desai, P. B., Cabrera, O. A. and Pazour, G. J. (2021). E3 ubiquitin ligase Wwp1 regulates ciliary dynamics of the Hedgehog receptor Smoothened. *J. Cell Biol.* **220**, e202010177. doi:10.1083/jcb.202010177
- Marín, I. and Ferrús, A. (2002). Comparative genomics of the RBR family, including the Parkinson's disease-related gene parkin and the genes of the ariadne subfamily. *Mol. Biol. Evol.* **19**, 2039-2050. doi:10.1093/oxfordjournals.molbev.a004029
- Marteijn, J. A., van Emst, L., Erpelink-Verschueren, C. A., Nikoloski, G., Menke, A., de Witte, T., Lowenberg, B., Jansen, J. H. and van der Reijden, B. A. (2005). The E3 ubiquitin-protein ligase Triad1 inhibits clonogenic growth of primary myeloid progenitor cells. *Blood* **106**, 4114-4123. doi:10.1182/blood-2005-04-1450
- Milenkovic, L., Scott, M. P. and Rohatgi, R. (2009). Lateral transport of Smoothened from the plasma membrane to the membrane of the cilium. *J. Cell Biol.* **187**, 365-374. doi:10.1083/jcb.200907126
- Mladek, C., Guger, K. and Hauser, M. T. (2003). Identification and characterization of the ARIADNE gene family in Arabidopsis. A group of putative E3 ligases. *Plant Physiol.* **131**, 27-40. doi:10.1104/pp.012781
- Nedelcu, D., Liu, J., Xu, Y., Jao, C. and Salic, A. (2013). Oxysterol binding to the extracellular domain of Smoothened in Hedgehog signaling. *Nat. Chem. Biol.* **9**, 557-564. doi:10.1038/nchembio.1290
- Olzmann, J. A., Kopito, R. R. and Christianson, J. C. (2013). The mammalian endoplasmic reticulum-associated degradation system. *Cold Spring Harb. Perspect Biol.* **5**, a013185. doi:10.1101/cshperspect.a013185
- Oslowski, C. M. and Urano, F. (2011). Measuring ER stress and the unfolded protein response using mammalian tissue culture system. *Methods Enzymol.* **490**, 71-92. doi:10.1016/B978-0-12-385114-7.00004-0
- Otten, E. G., Werner, E., Crespillo-Casado, A., Boyle, K. B., Dharamdasani, V., Pathe, C., Santhanam, B. and Randow, F. (2021). Ubiquitylation of lipopolysaccharide by RNF213 during bacterial infection. *Nature* **594**, 111-116. doi:10.1038/s41586-021-03566-4
- Pusapati, G. V., Kong, J. H., Patel, B. B., Krishnan, A., Sagner, A., Kinnebrew, M., Briscoe, J., Aravind, L. and Rohatgi, R. (2018). CRISPR screens uncover genes that regulate target cell sensitivity to the morphogen sonic hedgehog. *Dev. Cell* **44**, 271. doi:10.1016/j.devcel.2018.01.002
- Rausch, T., Fritz, M. H., Untergasser, A. and Benes, V. (2020). Tracy: basecalling, alignment, assembly and deconvolution of sanger chromatogram trace files. *BMC Genomics* **21**, 230. doi:10.1186/s12864-020-6635-8
- Rusilowicz-Jones, E. V., Brazel, A. J., Frigenti, F., Urbe, S. and Clague, M. J. (2021). Membrane compartmentalisation of the ubiquitin system. *Semin. Cell Dev. Biol.*, S1084-9521(21)00292-5.
- Sanjana, N. E., Shalem, O. and Zhang, F. (2014). Improved vectors and genome-wide libraries for CRISPR screening. *Nat. Methods* **11**, 783-784. doi:10.1038/nmeth.3047
- Suzuki, J., Kanemaru, K., Ishii, K., Ohkura, M., Okubo, Y. and Iino, M. (2014). Imaging intraorganellar Ca<sup>2+</sup> at subcellular resolution using CEPIA. *Nat. Commun.* **5**, 4153. doi:10.1038/ncomms5153
- Tang, J., Hu, M., Lee, S. and Roblin, R. (2000). A polymerase chain reaction based method for detecting Mycoplasma/Acholeplasma contaminants in cell culture. *J. Microbiol. Methods* **39**, 121-126. doi:10.1016/S0167-7012(99)00107-4
- Wang, H., Bei, L., Shah, C. A., Horvath, E. and Eklund, E. A. (2011). HoxA10 influences protein ubiquitination by activating transcription of ARIH2, the gene encoding Triad1. *J. Biol. Chem.* **286**, 16832-16845. doi:10.1074/jbc.M110.213975
- Wang, Q., Li, L. and Ye, Y. (2008). Inhibition of p97-dependent protein degradation by Eeyarestatin I. *J. Biol. Chem.* **283**, 7445-7454. doi:10.1074/jbc.M708347200
- Watanabe, T., Seki, T., Fukano, T., Sakaue-Sawano, A., Karasawa, S., Kubota, M., Kurokawa, H., Inoue, K., Akatsuka, J. and Miyawaki, A. (2017). Genetic visualization of protein interactions harnessing liquid phase transitions. *Sci. Rep.* **7**, 46380. doi:10.1038/srep46380
- Wilson, A. A., Kwok, L. W., Hovav, A. H., Ohle, S. J., Little, F. F., Fine, A. and Kotton, D. N. (2008). Sustained expression of alpha1-antitrypsin after transplantation of manipulated hematopoietic stem cells. *Am. J. Respir. Cell Mol. Biol.* **39**, 133-141. doi:10.1165/rcmb.2007-0133OC
- Xia, Y., Li, K., Li, J., Wang, T., Gu, L. and Xun, L. (2019). T5 exonuclease-dependent assembly offers a low-cost method for efficient cloning and site-directed mutagenesis. *Nucleic Acids Res.* **47**, e15. doi:10.1093/nar/gky1169
- Zhang, C., Williams, E. H., Guo, Y., Lum, L. and Beachy, P. A. (2004). Extensive phosphorylation of Smoothened in Hedgehog pathway activation. *Proc. Natl. Acad. Sci. USA* **101**, 17900-17907. doi:10.1073/pnas.0408093101

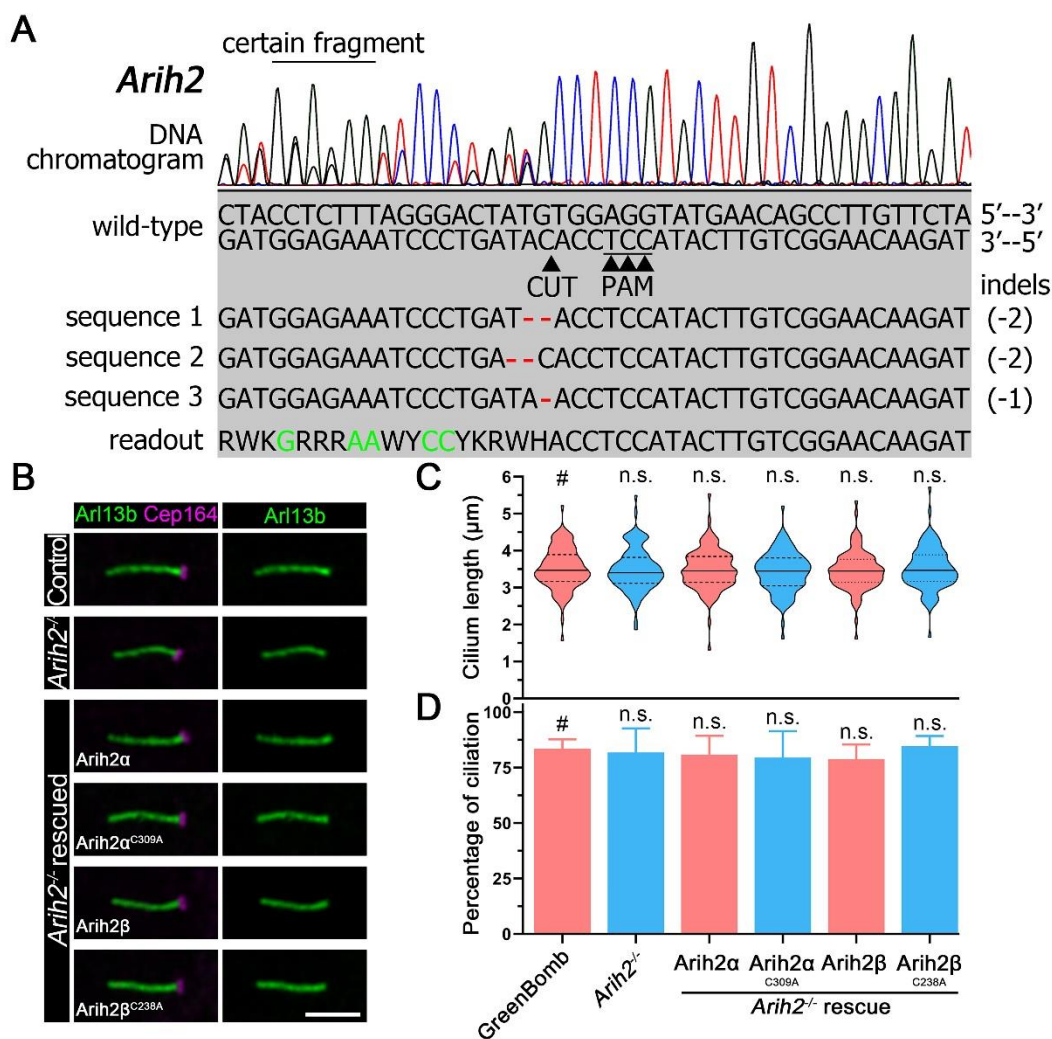


Figure S1

**Fig. S1. Arih2 knockout doesn't affect ciliogenesis.**

**A.** Chromatogram showing one typical clone (gOC173 C1) of *Arih2*<sup>-/-</sup> cell with deconvolved sequence. Red dashes mark deletions. Green letters in the sequence means defined bases in the readout.

**B.** Immunofluorescence of control, *Arih2*<sup>-/-</sup>, and *Arih2*<sup>-/-</sup> cells rescued with Myc-tagged *Arih2* $\alpha$  and *Arih2* $\beta$  along with the enzymatic dead versions *Arih2* $\alpha$ <sup>C309A</sup> and *Arih2* $\beta$ <sup>C238A</sup> stained for cilia (Arl13b, green) and basal bodies (Cep164, magenta). Scale bar, 3 microns.

**C.** Quantification of ciliary length in *Arih2*<sup>-/-</sup> and rescue cells. n = 100 repeats. n.s., not significant by One-Way ANOVA as compared to control (GreenBomb, labeled with #).

**D.** Quantification of percent ciliation in *Arih2*<sup>-/-</sup> and rescue cells. n = 5 repeats. n.s., not significant by One-Way ANOVA as compared to control (GreenBomb, labeled with #).

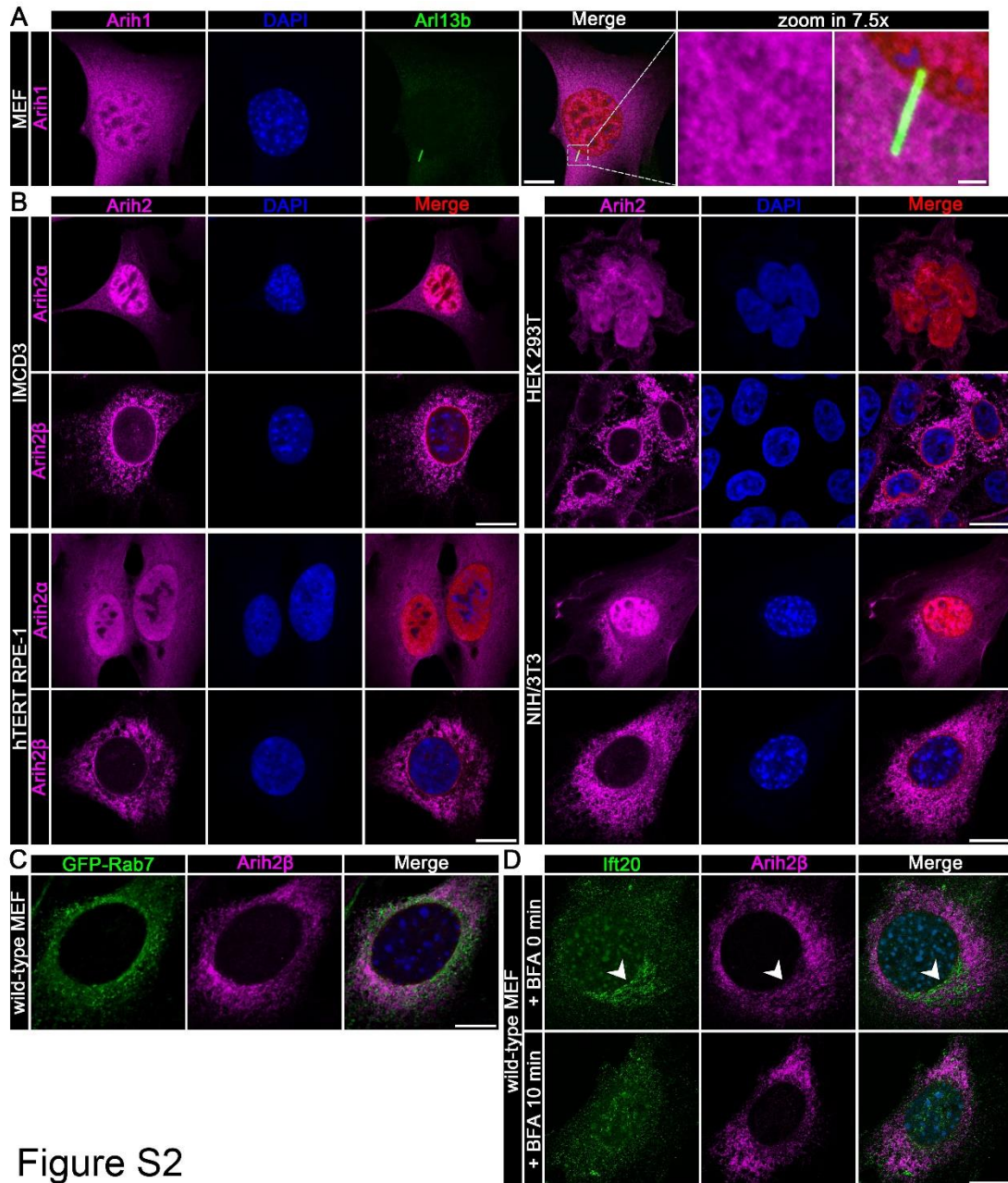


Figure S2

**Fig. S2. Aih2 $\alpha$  and Aih2 $\beta$  localization in diverse cell lines.**

- A.** Wild-type MEF cells expressing Flag-tagged Aih1 (BL1046) were stained for Aih1 (Flag, magenta), cilia (Arl13b, green), and DNA (DAPI, blue). Scale bar, 5 microns in original images and 1 micron in enlarged images.
- B.** IMCD3, HEK 293T, hTERT RPE-1, and NIH/3T3 cells transfected with Flag-tagged Aih2 $\alpha$  (BL225) and Aih2 $\beta$  (BL905) and stained for Aih2 (Flag, magenta) and DNA (DAPI, blue). Scale bar, 5 microns.
- C.** Wild-type MEF cells expressing Flag-tagged Aih2 $\beta$  (BL905) and GFP-Rab7 (BL1086) stained for Aih2 (Flag, magenta) and GFP (green). Scale bar, 5 microns.
- D.** Wild-type MEF cells expressing Flag-tagged Aih2 $\beta$  (BL905) were stained for Aih2 (Flag, magenta) and Ift20 (green) before and after treatment with BFA. Note that BFA disperses the Ift20 pool but not the Aih2 $\beta$  pool. Scale bar, 5 microns.

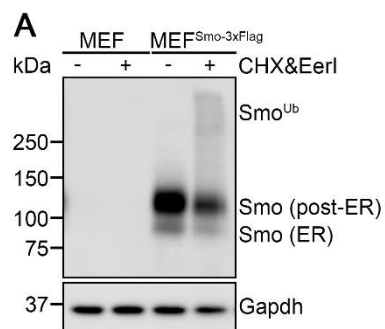


Figure S3

**Fig. S3. EerI treatment promotes the production of high molecular weight forms of Smo.**

**A.** Anti-Flag western blot of Wild type MEFs and MEF<sup>Smo-3xFlag</sup> either untreated or treated with cycloheximide (CHX) and EerI. Note large ubiquitinated forms of Smo when treated with CHX and EerI.

**Table S1. Plasmids.**

Name	Description	Promoter	Tags	Drug
#52961	lentiCRISPR v2 Puro	EF1 $\alpha$ ; U6	Flag	Puro
#58215	pCMV G-CEPIA1er	CMV	Myc	Neo
BL225	Arih2 $\alpha$ -3xFlag (492aa)	EF1 $\alpha$	Flag	Bsd
BL243	HsSHH	CMV	None	Puro
BL244	XtScube2-3xFlag	EF1 $\alpha$	Flag	Bsd
BL245	lentiCRISPR v2 Puro <sup>P93S</sup>	EF1 $\alpha$ ; U6	Flag	Puro <sup>P93S</sup>
BL256	Arih2 $\alpha$ -6xMyc (492aa)	CMV	Myc	Zeo
BL323	MmDisp1-6xMyc	CMV	Myc	Zeo
BL368	Arih2 $\alpha$ <sup>C309A</sup> -6xMyc (492aa)	CMV	Myc	Zeo
BL905	Arih2 $\beta$ -3xFlag (421aa)	EF1 $\alpha$	Flag	Bsd
BL929	Arih2 $\beta$ -6xMyc (421aa)	CMV	Myc	Puro
BL930	Arih2 $\beta$ <sup>C238A</sup> -6xMyc (421aa)	CMV	Myc	Puro
BL1035	3xTy1-Ub	CMV	Ty1	Neo
BL1046	Arih1-3xFlag	EF1 $\alpha$	Flag	Bsd
BL1086	GFP-MmRab7	CMV	GFP	Puro
BL1087	Syvn1-2xHA	CMV	HA	Puro
BL1099	ER-GFP (lysozyme-GFP-KDEL)	CMV	GFP	Puro
BL1117	Arih2 $\beta$ -GFP	EF1 $\alpha$	Flag	Bsd
BL1118	GFP-Arih2 $\beta$	EF1 $\alpha$	Flag	Bsd
BL1137	Arih2 knock in donor template	N.A.	Flag-Avi	Puro
BL1139	Arih2 knockout gRNA 3 GCACAGCCACAGCCAGTTT <sup>^</sup> AGG	EF1 $\alpha$ ; U6	Flag	Puro
BL1155	Arih2 $\beta$ -6xMyc (421aa)	CMV	Myc	Puro
BL1156	Arih2 $\beta$ <sup>C238A</sup> -6xMyc (421aa)	CMV	Myc	Puro
BL1192	Arih2 $\beta$ $\Delta$ 21-66	EF1 $\alpha$	Flag	Bsd
BL1194	Arih2 $\beta$ $\Delta$ 48-66	EF1 $\alpha$	Flag	Bsd
BL1195	Arih2 $\beta$ $\Delta$ 41-66	EF1 $\alpha$	Flag	Bsd
BL1196	Arih2 $\beta$ $\Delta$ 30-66	EF1 $\alpha$	Flag	Bsd
BL1203	Smo-3xFlag-Avi	CMV <sup>weak</sup>	Flag-Avi	Bsd
BL1206	Arih1-6xMyc	CMV	Myc	Puro
BL1207	Arih2 $\beta$ $\Delta$ 22-66	EF1 $\alpha$	Flag	Bsd
BL1208	Arih2 $\beta$ $\Delta$ 23-66	EF1 $\alpha$	Flag	Bsd
BL1209	Arih2 $\beta$ $\Delta$ 24-66	EF1 $\alpha$	Flag	Bsd
BL1210	Arih2 $\beta$ $\Delta$ 25-66	EF1 $\alpha$	Flag	Bsd
BL1211	Arih2 $\beta$ $\Delta$ 26-66	EF1 $\alpha$	Flag	Bsd
BL1212	Arih2 $\beta$ $\Delta$ 27-66	EF1 $\alpha$	Flag	Bsd
BL1213	Arih2 $\beta$ $\Delta$ 28-66	EF1 $\alpha$	Flag	Bsd
BL1214	Arih2 $\beta$ $\Delta$ 29-66	EF1 $\alpha$	Flag	Bsd
BL1217	Arih2 $\beta$ $\Delta$ N22	EF1 $\alpha$	Flag	Bsd
BL1218	N22-GFP-Arih2 $\beta$	EF1 $\alpha$	Flag	Bsd
BL1219	Arih2 $\beta$ N22-GFP	EF1 $\alpha$	Flag	Bsd
BL1231	AG-PB1	EF1 $\alpha$	Flag	Bsd
BL1232	Smo-PB1	CMV	Flag	Bsd
BL1233	Arih2 $\beta$ -3xAG	EF1 $\alpha$	Flag	Bsd
BL1234	Arih2 $\alpha$ -AG	EF1 $\alpha$	Flag	Bsd

BL1239	AG	EF1 $\alpha$	Flag	Bsd
BL1253	Smo $\Delta$ CT-PB1	CMV	Flag	Bsd
BL1254	Arih2 $\beta$ $\Delta$ Ariadne-AG	EF1 $\alpha$	Flag	Bsd
BL1255	Arih2 $\beta$ $\Delta$ TRIAD-AG	EF1 $\alpha$	Flag	Bsd
BL1257	G-CEPIA1-ER	EF1 $\alpha$	Flag	Bsd
BL1258	G-CEPIA1	EF1 $\alpha$	Flag	Bsd
BL1261	Arih2 $\beta$ -G-CEPIA	EF1 $\alpha$	Flag	Bsd
BL1262	G-CEPIA-Arih2 $\beta$	EF1 $\alpha$	Flag	Bsd
BL1263	Smo-3xFlag-GFP-IRES2-mCherry	CMV <sup>weak</sup>	Flag, GFP	None
GP778	8xGliBox-GgCryD1-nucGFP	Gli	NLS	Nat
OC166	lentiCRISPR v2 Nat	EF1 $\alpha$ ; U6	Flag	Nat
OC173	Arih2 knockout gRNA 1 CCTCTTTAGGGACTATG <sup>^</sup> TGG	EF1 $\alpha$ ; U6	Flag	Puro
OC174	Arih2 knockout gRNA 2 GCAGTGCAATCGGTGCA <sup>^</sup> GCG	EF1 $\alpha$ ; U6	Flag	Puro
PD22	Smo-3xFlag	CMV	Flag	Bsd

**Table S2. Antibodies.**

<b>Immunogen</b>	<b>Clone name</b>	<b>Dilution</b>	<b>Supplier</b>	<b>Catalog number/Reference</b>
Arl13b	N295B/66	1:1000	Davis/NIH NeuroMab	75-287
Cep164	N.A.	1:1000	Proteintech	22227-1-AP
Flag	M2	1:1000	Sigma	F1804
Gapdh	14C10	1:5000	Cell Signaling Technology	#3683S
GFP	N.A.	1:1000	Sigma	G1544
GFP	3E6	1:1000	Thermo Fisher Scientific	A-11120
Ift20	N.A.	1:1000	lab made	(Follit et al., 2006)
Mouse IgG (HRP)	N.A.	1:10000	Thermo Fisher Scientific	31432
Mouse IgG1 (488)	N.A.	1:1000	Thermo Fisher Scientific	A-21121
Mouse IgG1 (568)	N.A.	1:1000	Thermo Fisher Scientific	A-21124
Mouse IgG2a (488)	N.A.	1:1000	Thermo Fisher Scientific	A-21131
Mouse IgG2a (568)	N.A.	1:1000	Thermo Fisher Scientific	A-21134
Myc	9E10	1:1000	Sigma	M4439
Rabbit IgG (488)	N.A.	1:1000	Thermo Fisher Scientific	A-21206
Rabbit IgG (568)	N.A.	1:1000	Thermo Fisher Scientific	A-11011
Rabbit IgG (HRP)	N.A.	1:10000	Thermo Fisher Scientific	31460
Ty1	BB2	1:1000	Thermo Fisher Scientific	MA5-23513



**Table S3. PCR, RT-PCR and Quantitative RT-PCR primers.**

Primer	Accession No.	Sequence	Tm	Length
ATF4_F	ENSMUSG00000042406	GGGTTCTGTCTTCCACTCCA	60	96
ATF4_R	ENSMUSG00000042406	AAGCAGCAGAGTCAGGCTTTC	60	96
Ddit3_F	ENSMUSG00000025408	CCACCACACCTGAAAGCAGAA	60	67
Ddit3_R	ENSMUSG00000025408	AGGTGAAAGGCAGGGACTCA	60	67
Gapdh_F	NM_008084	GCAATGCATCCTGCACCACCA	61.1	138
Gapdh_R	NM_008084	TTCCAGAGGGGCCATCCACA	61.1	138
Hsp90b1_F	ENSMUSG00000020048	AAGAATGAAGGAAAAACAGGAAAA	60	77
Hsp90b1_R	ENSMUSG00000020048	CAAATGGAGAAGATTCCGCC	60	77
Hspa5_F	ENSMUSG00000026864	TTCAGCCAATTATCAGCAAACCTCT	60	73
Hspa5_R	ENSMUSG00000026864	TTTTCTGATGTATCCTCTTACCAGT	60	73
MmGli1_F	NM_010296	CTCGACCTGCAAACCGTAATC	60	126
MmGli1_R	NM_010296	TCCTAAAGAAGGGCTCATGGTA	60	126
OC173_F	knockout sequencing	AAAGGTGCCACCATACCCAG	59	475
OC173_R	knockout sequencing	AGGTGCCTAGAAGAGCCAGA	59	475
OC174_F	knockout sequencing	GTAAGCCGTCAACTGGGAGT	59	307
OC174_R	knockout sequencing	CTCTTCTAGACACGTGCGCC	59	307
Primer 1	<i>Arih2</i>	CCTGGTTTGGTCTGGCTTGA	60	329
Primer 2	<i>Arih2</i>	GTCCTCTATGTCCCCAGGGT	60	329
Primer 3	<i>Arih2</i>	GTCAGCCTGGTTTGGTCTGG	60	708
Primer 4	<i>Arih2</i>	CGGCAAAACTGATGTTGGCA	60	708
Primer 5	<i>Arih2</i>	TCTGCAACTTTGCTGGATGTT	60	506
Primer 7	<i>Arih2</i>	TTCTGCAACTTTGCTGGATGT	60	672
Primer 8	<i>Arih2</i>	TCCCTAAAGAGGTAGCGCCT	60	672
Smo_For2	NM_176996	GACTCCGTGAGTGGCATCTG	59	261
Smo_Rev2	NM_176996	GTGGCAGCTGAAGGTGATGA	58	261
sXBP1_F	ENSMUSG00000020484	CTGAGTCCGAATCAGGTGCAG	60	59
usXBP1_F	ENSMUSG00000020484	CAGCACTCAGACTATGTGCA	60	76
XBP1_F	ENSMUSG00000020484	TGGCCGGGTCTGCTGAGTCCG	60	97
XBP1_R	ENSMUSG00000020484	GTCCATGGGAAGATGTTCTGG	60	97
Guide1_F	<i>Arih2</i> KO	CACCGCCTCTTTAGGGACTATGATG	N.A.	N.A.
Guide1_R	<i>Arih2</i> KO	AAACCATCATAGTCCCTAAAGAGGC	N.A.	N.A.
Guide2_F	<i>Arih2</i> KO	CACCGGCAGTGCAATCGGTGCAGCA	N.A.	N.A.
Guide2_R	<i>Arih2</i> KO	AAACTGCTGCACCGATTGCACTGCC	N.A.	N.A.
Guide3_F	<i>Arih2</i> KO for KI	CACCGGCACAGCCACAGCCCAGTTT	N.A.	N.A.
Guide3_R	<i>Arih2</i> KO for KI	AAACAAACTGGGCTGTGGCTGTGCC	N.A.	N.A.
Myc_F	mycoplasma detection	ACACCATGGGAGCTGGTAAT	66	350-
Myc_R	mycoplasma detection	CTTCWTCGACTTYCAGACCCAAGGCA	71	500